Detachment fold vs. ramp anticline: a gravity survey in the southern Pyrenean front (External Sierras)

Pablo Calvín[a,b], Pablo Santolaria[b], Antonio M. Casas[b], Emilio L. Pueyo[c,d]

[a] Departamento de Física, Universidad de Burgos, Av/ Cantabria, s/n, 09006 Burgos, Spain.

[b] Departamento de Ciencias de la Tierra, Universidad de Zaragoza, C/Pedro Cerbuna, 12, 50009 Zaragoza, Spain.

[c] Instituto Geológico y Minero de España, Unidad de Zaragoza, C/Manuel Lasala 44, 9B, 50006 Zaragoza, Spain.

[d] Unidad Asociada en Ciencias de la Tierra IGME. Universidad de Zaragoza.

Corresponding author. Pablo Calvín (pcalvin@ubu.es). (+34) 690 789 887. Departamento de Física, Universidad de Burgos, Av/ Cantabria, s/n, 09006 Burgos, Spain.

Abstract

The Santo Domingo Anticline (External Sierras, Southern Pyrenees), which separates the Jaca piggyback basin from the Ebro foreland basin, is a key structure of the Pyrenees. Its geometry has been interpreted both as a detachment fold and as a hangingwall anticline associated with an underlying thrust. In this paper, we present the results from a gravity survey and 2.5D gravity modeling carried out around the Santo Domingo Anticline. Density measurements indicate a sharp density contrast between the Triassic evaporites-mudstones in the core of the anticline and the sedimentary sequence (limestones and sandstones) at its limbs. Gravity anomalies together with 2.5D gravity models allow to discern the along-strike structural

changes. From east to west we document a change from the ramp-associated fold to the detachment anticline. The capabilities and limitations of the gravimetric method for the determination of fold geometry are also discussed.

Keywords

Detachment fold; hangingwall anticline; Bouguer anomaly; 2.5D gravity modelling; Southern Pyrenees.

Highlights

New gravity and density data from the Southern Pyrenees.

A WNW-ESE, gravity low and a dipolar anomaly characterize the Santo Domingo Range.

2.5 D Gravity models point out to an along-trend change in fold geometry. A change in the gravity trend reveals structural subsurface changes.

Symmetry of the gravity signal reflects symmetries of the subsurface structure.

1. INTRODUCTION

Understanding the underground geometry of some geological scenarios is not always easy. In some cases, geophysical exploration cannot be successfully applied because of the boundary conditions of the problem (e.g. dip of beds, contrasts of physical properties and depth to the target) and the limited resolution of the applied method(s). For example, the reconstruction of fold having sub-vertical limbs is difficult using reflection seismic (Sheriff and Geldart, 1995). Therefore, when certain geophysical surveying methods cannot be applied, modern

techniques for building and balancing cross sections (Woodward *et al*., 1991 and references therein) may shed some light. Giving a great importance to geological mapping and honoring some basic geometrical rules (e.g. preservation of area, length and thickness of sedimentary sequences) in fact, they will guarantee a potentially correct 2D reconstruction of the underground (Dahlstrom, 1969). However, cross section balancing does not often give a univocal solution to the problem, and alternative solutions may also fulfill the starting conditions. Cross-section balancing, often combined with geophysical data, has demonstrated its utility in the reconstruction of the structure of fold-and-thrust belts (e.g. Beauchamp *et al*., 1999).

Fold-and-thrust belts may develop under a large variety of kinematic settings and may display a wide range of resulting geometries depending upon a number of variables including for example: (i) stratigraphy (e.g. Massoli *et al*., 2006; Konstantinovskaya and Malavielle, 2011; Santolaria *et al*., 2014), pre-compressional basin geometry (e.g. Soto *et al*., 2002, 2003) and mechanical properties of the rocks (e.g. Lohrmann *et al*., 2003; Nilfouroushan *et al*., 2011), (ii) inherited anisotropies, (iii) shortening directions (e.g. Richard and Cobbold, 1989; Soto *et al*., 2006), (iv) convergence rates (e.g. Cousenz-Schultz *et al*., 2003; Smit *et al*., 2003) and (v) syntectonic erosion and sedimentation processes (e.g. Gestain *et al*., 2004; McClay and Whitehouse, 2004; Fillon *et al*., 2013). When dealing with folded geometry, the above mentioned variables and the kinematics of deformation may produce very different end-member structures, including fault-propagation folds, fault-bend folds or detachment folds (Suppe, 1983; Mitra, 1990; Suppe and Medwedeff, 1990; Jamison, 1992; Epard and Groshong, 1995; Homza and Wallace, 1995).

Because of their spectacular outcrop conditions and preservation of syn-tectonic sediments, the Pyrenees have been the target of numerous structural studies concerning the development of fold-and-thrust belts (e.g. Millán *et al.*, 2000 and references therein).

Particularly, the structural configuration of the southwesternmost sector of the Southern Pyrenean front (External Sierras, Fig. 1a) was object of discussion about its geometry and kinematics, with two end-member solutions: detachment fold and ramp anticline. The External Sierras fold-and-thrust belt laterally ends in a kilometric-scale fold having abnormally high amplitude (5 km minimum) and nearly vertical, parallel flanks: the Santo Domingo Anticline (Nichols, 1984; Turner, 1988; Millán, 1996) (Figs. 1b, 2). Although seismic profiles were performed in the areas surrounding the anticline, its vertical flanks have precluded the use of this technique for the interpretation of the geometry of its core. Consequently, a unique interpretation of the underground geometry was never reached and the anticline was interpreted according to three different models: (1) the detachment fold (DF) model, with a large evaporitic core of Triassic rocks that laterally becomes a thrust ramp to the east (Millán *et al*., 1995 and Millán, 1996); (2) a mixed model of fault propagation and detachment fold with a large thrust ramp underneath (RA model, Teixell and García-Sansegundo, 1995; Teixell, 1996). It is worth mentioning that both end-members are balanced and geometrically plausible and (3) diapirism and salt tectonics model (Anastasio, 1992).

In the External Sierras, gravity surveying may help choosing the most feasible underground geometry of the Santo Domingo Anticline. Application of gravimetry can help to recognize anomalies produced by the low-density evaporites (Pinto and Casas, 1996; Sarsar-Naouali *et al*., 2011; Santolaria *et al*., 2014) and, by means of modeling techniques, to discern the geometry of its deep structure. Based on a new gravity anomaly map derived from five densely sampled gravity sections along- and across-strike the anticline and 2.5D gravity modeling technique, we aim to test the reliability of subsurface structural interpretations of the Santo Domingo Anticline.

2. GEOLOGICAL SETTING

The Pyrenees derived from the continental collision between the Iberian and the Eurasian plates occurred from Late Cretaceous to Miocene times. The Pyrenean orogenic wedge displays an asymmetric, double-verging geometry (Muñoz, 1992). In the Southern Pyrenees (west of the South Pyrenean Central Unit; Séguret, 1972) (Fig. 1) the structural units show a dominant southward motion (Fig. 1). The Axial Zone (backbone of the chain), where the Paleozoic rocks and the Late Carboniferous-Permian granites crop out, is bounded to the south by the Internal Sierras (Séguret, 1972; Labaume *et al*., 1985; Izquierdo-Llavall *et al*., 2013) (Fig. 1b), whose sedimentary sequence (Upper Cretaceous to Paleocene limestones) was deformed during the Eocene-Miocene Pyrenean compression. To the south of the Internal Sierras, the Eocene turbiditic sequences (Mutti *et al*., 1988) and the molassic rocks of the Jaca piggyback basin (Puigdefàbregas, 1975) define the Guarga synclinorium, caused by the stacking of basement units underneath the Axial Zone and the ramping of the basal Pyrenean thrust to the south (Fig. 1b). The southern limb of the Guarga synclinorium forms the External Sierras, that represent the emergence at the topographic surface of the Pyrenean sole thrust, separating the Jaca piggyback basin in the north, from the Ebro foreland basin in the south (Fig. 1a) (Mallada, 1878; Almera and Ríos, 1951; Puigdefàbregas and Soler, 1973; Nichols, 1984; Ori and Friend, 1984; McElroy, 1990; Anastasio, 1992; Millán *et al*., 1995; Teixell and García-Sansegundo, 1995).

Although the onset of contractional tectonics in the north-central portion of the Pyrenean belt is of Late Cretaceous age (Puigdefàbregas and Souquet, 1986; Choukroune *et al*., 1989; Muñoz, 1992), in the western Pyrenees only the Lakora thrust system is consistent with this Late Cretaceous deformation age. Conversely, the main episodes of deformation in the southwestern sector took place during the Eocene-Miocene in relation to the emplacement of the Gavarnie (outcropping in the north) and Guarga (underneath the Jaca Basin) basement

thrust sheets (Teixell, 1996, 1998; Casas and Pardo, 2004; Fig. 1). The timing of deformation in the region can be obtained from outstanding and well-dated syntectonic sequences related to the progression of folding and thrusting of the cover units to the south of the Axial Zone and particularly in the External Sierras (Teixell, 1998; Millán *et al*., 2000; Martínez-Peña and Casas-Sainz, 2003; Hogan and Burbank, 1996; Oliva-Urcia *et al*., 2016).

2.1. The External Sierras

2.1.1. Stratigraphy

Focusing on the stratigraphy of the External Sierras, Upper and Middle Triassic evaporites crop out in the lowest part of the well-exposed stratigraphic section (Fig. 2a). They are composed by gypsiferous mudstones and dolostones uncomformably overlain by a thinned sequence of Upper Cretaceous sandstones and limestones (Adraen-Bona Fm.) and Garumnian fluvial and lacustrine facies (Tremp Fm.). The shallow carbonate succession of the Guara Fm. represents the Lutetian platform covering a significant part of the South Pyrenean Basin (Barnolas and Gil-Peña, 2001) and constitutes a main cartographic level at the base of the Cenozoic stratigraphic succession. In the western and central portions of the External Sierras, these Eocene carbonate deposits grade into the Arguis Fm. (Bartonian-Priabonian), consisting of azoic blue marls from outer ramp areas interbedded with shallow siliciclastic and carbonate facies from middle and inner ramp areas. The synorogenic deltaic sequences of the Belsué-Atarés Fm. (absent in the study area) span from Latest Lutetian to the Early Priabonian and thin significantly to the west passing to the Yeste-Arrés Fm. This part of the Mesozoic and Cenozoic pile hardly reaches 500 m in thickness in the study area in contrast with the continental synorogenic strata, the Campodarbe Fm., that define a 3000 to 4000 m thick fluvial monotonous succession (Upper Eocene to Oligocene). Finally, the conglomerates,

sandstones and siltstones of the Uncastillo and Bernués Fms. (deposited from Middle to Late Miocene, Oliva-Urcia *et al*., 2016) form the top of the sequence (≈ 1300 m). This formation surrounds the southern edge of the External Sierras and lie uncomformably on the former lithostratigraphic units, recording the last age compressive events in the region

2.1.2. Geometry and kinematics

The External Sierras is an imbricate fold and thrust system displaying a main structural WNW-ESE trend along more than 100 km. Thrust sheets emplacement took place from Middle Eocene to Early Miocene in two main deformation episodes, testified by synorogenic deposits (Puigdefàbregas, 1975; Arenas, 1993; Hogan and Burbank, 1996; Millán *et al*., 2000; Arenas *et al*., 2001). The first one is related to the age emplacement of the Gavarnie basement thrust sheet (Fig. 1b) and its subsequent propagation toward the south through Mesozoic detachment levels into the cover rocks of the undeformed foreland basin. At that time, the thin cover (500-1000 m) of Mesozoic-Cenozoic rocks favored the development of short wavelength folds and closely spaced thrusts sheets within the imbricate system. The deformation ages for these fold-and-thrust systems are derived from syntectonic sedimentation that witness a remarkable diachronism of more than 30 Ma (Millán *et al.*, 2000) with progressively younger ages of deformation toward the west. The second deformation episode took place during Miocene times in relation to the movement of the Guarga basement thrust underlying the Jaca Basin (Fig. 1b). The southern tip of the Guarga thrust cut across a thick Cenozoic cover (up to 5 km), thus separating the Ebro Basin (to the south) from the Jaca piggyback basin (to the north) (Fig. 1b). During the second stage, deformation was quicker and the entire South Pyrenean basal thrust system moved almost synchronously (Millán *et al*., 2000). This two-stage evolution is responsible for the remarkable pattern of transverse and

oblique structures (N-S to NW-SE) superimposed on the main WNW-ESE tectonic grain of the mountain chain (e.g. Mallada, 1878; Almera and Ríos, 1951) (Fig. 1). The superposed folding is partially caused by moderate-strong vertical axis rotations related to the movement of the basal thrust in the External Sierras (Pueyo *et al.*, 2004; Mochales *et al.*, 2012; Rodríguez-Pintó *et al.*, 2016).

2.2. The Santo Domingo Anticline

The Santo Domingo Anticline is the most significant structure in the western sector of the External Sierras (Fig. 2) that developed during the second deformation stage. It is a 20 km long anticline trending WNW-ESE and detached along the incompetent Middle and Upper Triassic levels (Nichols, 1984, 1987; Turner, 1992; Millán, 1996). The Santo Domingo Anticline was active during the Late Oligocene-Early Miocene as attested by syntectonic sedimentation along the southern flank of the fold (Puigdefàbregas, 1975; Millán *et al.*, 1995; Arenas *et al.*, 2001). The syntectonic sequence has been dated by magnetostratigraphic methods (Hogan and Burbank, 1996; Oliva-Urcia *et al.*, 2016) giving a refined chronostratigraphic frame to the deformation history of the fold. There are several interpretations on its depth geometry (and related kinematic evolution). Some authors (Millán *et al.*, 1995) interpret its geometry as a large-scale detachment conical flexural fold, having parallel and near-vertical limbs (the DF model) (Fig. 2b). Others (Nichols, 1987; Teixell and García-Sansegundo, 1995; Teixell, 1996) proposed a cylindrical fold related to an underneath thrust ramp (the RA model) (Fig. 2b) or a footwall ramp stacking (duplex structure, Hervouët *et al.*, 2005). To the south of the anticline, some structural elements were interpreted as a result of backthrusting (Nichols, 1987; Turner, 1992) while a recumbent fold is invoked in other interpretations (Millán *et al.*, 1995; Teixell and García-Sansegundo, 1995).

3. Methodology

3.1. Gravity survey

During the gravity survey a total of 233 new gravity measurements were taken within an area of 900 km^2 (Fig. 3a). The location of the measurement sites was conditioned by the rugged landscape, the site accessibility and the geological target. Stations are separated about 1 km close to the core of the Santo Domingo Anticline and about 3 km in the surrounding areas (i.e. in the Jaca Basin and in the Ebro foreland basin, Figs. 2 and 3). Stations were taken as far as 10 km away from the Santo Domingo Range (the geographical expression of the Santo Domingo Anticline) to refine the regional gravity signal and to avoid border effects in the anomaly maps. Site location (elevation and spatial positioning) was based on global positioning systems (GPS) and the available benchmark absolute altitude values from 1:25.000 scale topographic maps. Despite the accurate altitude absolute values (±0.01 m), GPS location allows to locate gravity station with metric accuracy around the absolute altitude. Where absolute altitudes were not available or technically unapproachable, differences in altitude with respect to reference benchmarks were measured with a barometric altimeter (with a claimed precision of ±0.15 m), always minimizing the time gap between measurements in order to avoid pressure changes. With all these procedures and considering nearly flat surfaces around the absolute altitude point, we can assume an altitude precision about 0.25 m (equivalent to 0.07 mGal).

Gravity readings were taken with a Lacoste-Romberg gravimeter (model G) and referred to the Spanish net for absolute gravity (REGA, Vaquero and Sainz-Maza, 2011) through the absolute gravity base located at the University of Zaragoza (g = 980.2241 cm/s^2; E 674983, N 4612328, alt. 225 m, ETRS89-30T zone). Additionally to the main base station,

measurements were systematically repeated in several relative bases. Observed values were corrected for effects caused by instrumental drift and earth tides.

Standards were used to obtain the Bouguer anomaly (Hinze *et al*., 2005). Theoretical gravity value was calculated following the theoretical ellipsoid based on the Geodetic Reference System (GRS80, Moritz, 1980). For height correction, we used the equation of LaFehr (1991) modified by Heiskanen and Moritz (1969). The Bouguer reduction considers the effect on the gravity of the Bouguer slab, having a density of 2560 kg/m^3 as derived from mean density measurements of rocks in this area (recommended methodology for local surveys, Hinze *et al*., 2005). Finally, the terrain correction takes into account the steep topography of the area. The Santo Doming Range is characterized by an elongated WNW-ESE relief. The highest land-surface altitude in the study area is 1524 m.a.s.l. and the lowest 800 m.a.s.l. within the Ebro Basin. A high-resolution digital terrain model with a 5 x 5 m grid (PNOA given by © Instituto Geográfico Nacional) was used to calculate the terrain correction based on the Hammer chart (Hammer, 1939; Tziavos *et al*., 2010). Terrain corrections were performed from an inner radius of 2 m to an outer radius of 300 km (thus near, medium and far topographic correction are considered). In the study area, terrain correction values range from 0.72 mGal to 15.85 mGal (see Supplementary Material). Bouguer anomaly values were obtained by subtracting the theoretical gravity to the observed gravity. These values range from -78.02 to –55.68 mGal (see Supplementary Material).

Bouguer anomaly was interpolated by minimum curvature (Fig. 3b). Its values result from the combination of short and long wavelength components of the gravity field, which corresponds to deep-seated and near-surface geological features, respectively. In order to study the near-surface structure (less than 5 km depth) where our target is located, it is necessary to subtract the regional trend (i.e. the factors associated with long wavelength anomalies) from the Bouguer anomaly. In our case, the regional trend-surface is related to the Moho depth that

deepens progressively towards the north (Casas *et al*., 1997).

Surface analysis applied to regional-residual separation involved the calculation of an optimum polynomial surface to match the Bouguer anomaly gravity field (Fig. 3b). Several regional anomaly surfaces considering different polynomial degrees were tested to evaluate its consistency with gravity trends found in the Pyrenean area and its validity to remove the regional trend (WNW-ESE, N-dipping surface) from the Bouguer anomaly. Then, the residual anomaly (Fig. 3c) was calculated by subtracting the best-fit polynomial surface from the Bouguer anomaly. In this case, the regional gravity anomaly was assimilated to a third-order surface.

3.2. Density measurements and 2.5D gravity modelling

Interpretation and 2.5D modelling of gravimetric anomalies are very sensitive to petrophysical properties of rocks (Henkel, 1976). Therefore, density values of 376 samples from the main geological units present in the Santo Domingo area were measured with a precision balance, calculating the volume of the sample from subtraction of the weight of the sample in air and water.

2.5D modelling of the residual anomaly was carried out with the Gravmag software (British Geological Survey, Pedley *et al.*, 1993) in two selected sections (Fig. 3a) perpendicular to the fold axis (Fig. 3c). The two end-member structural hypotheses (DF and RA models, Fig. 2b) were tested to contrast the modeled gravity anomaly and the residual gravity signal. The concept of the software is based on the definition of 2D polygons (X, Y axis) characterized by a finite length in the third dimension (Z axis) and a specific density value. Therefore, 2.5D model sections are constructed by substituting each geological body by a constant-density polygon. The 2.5D modeling is achieved by giving a length to each

polygon in the third dimension, perpendicular to the plane of the cross-section. Modeling is more accurate when cross sections are far from lateral terminations of structures because the software considers a symmetrical extension of the prisms to both sides of the section. Finally, the software models the contribution of these prisms to the gravity signal, which is plotted and compared with the measured gravity.

Workflow includes four main steps: (1) compilation of field data and geological map information, (2) acquisition of petrophysical data, (3) construction of geological cross section, (4) balancing of the gravimetric signal in the sections by means of 2.5D gravity modeling. Feedback in the workflow is needed to fit the modeled gravity response to the gravity measured in the field.

4. GRAVITY AND DENSITY DATA

The Bouguer anomaly map (Fig. 3b) shows a dominant WNW-ESE trend, parallel to the main structure, with values decreasing toward the NNE. This trend is interrupted in correspondence of the western termination of Santo Domingo Anticline, where lower gravity values depict a salient into a less negative area. This overall trend is consistent with the general Bouguer anomaly map of the Pyrenees (Casas *et al*., 1997; Ayala *et al*., 2016) related to the northward deepening of the Moho which is, at the same time, related to crustal thickening and/or the wedge-shaped infill of the South Pyrenean Basin (Casas *et al*., 1997).

The residual gravity map (Fig. 3c) reflects the gravity signal of the near-surface geological bodies. Residual anomaly values range from -7 mGal to 10 mGal. The residual gravity map (Fig. 3c) exhibits, as the main feature, a WNW-ESE elongated gravity low (-5 mGal) located between the center and the east of the study area. This gravity low shows a clear southern limit where gravity values increase regularly, reaching 0 mGal, whereas to the

north gradients are more variable and gravity values depict an unclear pattern. To the west, and aligned with the gravity low, a relative gravity high (3 mGal) appears, coinciding with the western end of the Santo Domingo Anticline. To the east of the main gravity low, the residual gravity anomaly becomes more complex: it splits into a secondary gravity low (-1.5 mGal) to the north and a gravity high to the south (3.5 mGal). The rest of the area is close to homogeneous 0 mGal residual gravity with the exception of some localized spots and boundary effect errors due to the interpolation process.

Laboratory density values are summarized in Figure 4 and Table 1. In the core of the anticline, Triassic rocks (evaporites and mudstones) present values around 2300 kg/m^3, whereas mean density of the interbedded Muschelkalk dolomites is 2675 kg/m^3. Host rocks attain values between 2600 and 2700 kg/m^3 in limestones and sandstones, respectively, and around 2500-2600 kg/m^3 in mudstones and marls, respectively. These values agree with other values obtained by works conducted in the South Pyrenean Zone (Santolaria *et al*., 2014), attesting a strong density contrast between the evaporitic Triassic rocks and the overlying cover formations.

5. 2.5D MODELING RESULTS

Gravimetric modeling was performed accompanied by a comprehensive analysis and interpretation of gravimetric maps. By means of this method, we modeled the structure in cross sections and observed the shape, amplitude, wavelength and symmetry of the gravimetric profiles within a vertical plane crossing through the main gravity low that coincides with the core of the Santo Domingo Anticline (see below). Instead of looking for the best-fit between the residual and the calculated values to perform an *ad hoc* model, we have observed variations in the amplitude and wavelength of gravimetric anomalies and

analyzed the response of the calculated gravity to changes in different parameters within the model (i.e. depth to the basement, volume of evaporites, geometry of the structure, etc.). The main differences between the end-members invoked to solve the geometry of the Santo Domingo Anticline (Fig. 2b) are the occurrence of a ramp underneath the anticline, the symmetry of the fold at depth and the volume of evaporites underlying the Cretaceous-Oligocene sedimentary sequence. These differences have significant implications in the associated gravimetric anomaly. We therefore constructed 2.5D models from two cross-sections oriented perpendicular to the Santo Domingo Anticline reflecting the two interpretations (Fig. 5).

Residual anomaly profile of the Western Section elaborated for both the RA and DF models (left column in Fig. 5a, b) depicts, from north to south, a decreasing trend broken by a minor gravity low (-1 mGal) and followed by a gravity high that attains 0 mGal. Towards the south, values drop to -3 mGal depicting the main gravity low. In the same direction, residual gravity values progressively increase up to 2 mGal and then they decrease gradually towards the Ebro Basin in the south. In a general view, gravity profiles are symmetric, with a central minimum and progressive increase towards the two branches of the curve. In the Eastern Section (Fig. 5c, d) the residual anomaly profile exhibits, from north to south, a decreasing trend that ends in the main gravity low (-2 mGal). Moving toward the south, residual gravity sharply increases up to 4 mGal and progressively decreases moving towards the Ebro basin. Observed gravity profile is asymmetric because of the different maximum values in the northern and southern branches located at both sides of the central gravity low.

Residual gravity anomaly profile displays a central gravity low located over the Santo Domingo Anticline in both the Eastern and Western sections but differences arise regarding the symmetry of the curve. Whereas in the Western Section (Fig. 5a, b) it shows a symmetric geometry, in the Eastern profile (Fig. 5c, d) it is markedly asymmetric. On the other hand, it is

important to discriminate between long- and short-wavelength anomalies (longer and shorter of 2-3 km, respectively). Smoothed shape of the residual gravity profile (i.e. the long-wavelength anomaly related to the core of the Santo Domingo Anticline and its amplitude) indicate that it is sourced in relatively deep-seated (more than 2 km depth) rather than shallow (less than 2 km depth) bodies. Superimposed on this overall trend, there are short-wavelength anomalies related to geological features located at shallow structural levels (less than 1-2 km)

We assume that, northwards and southwards of the Santo Domingo Anticline, the geological structure at depth is well constrained and its main features must be considered as inputs for modeling the gravity signal. Assuming that the mean density remains unchanged from surface down to 5 km (Santolaria *et al*., 2014), we tested the consistency of the two hypotheses regarding the subsurface geometry of the Santo Domingo Anticline.

In order to construct comparable models, consistency of the density values and basement geometry are needed. We used constant density calculated values of the non-evaporitic formations (Table 2) among all the models. Uncertainties arise regarding the Triassic rocks. First of all, Triassic rocks cropping out in the core of the anticline show variable and local significant thickness of dolomitic rocks interbedded within evaporites and mudstones (See M3 in Fig. 6). This package of dolostones is folded harmonically with the Mesozoic-Cenozoic overburden, as suggested by the consistency of outcrop patterns displayed on the geological map and field observations (Fig. 6). On the other hand, the RA and DF models suggest the thickening of the Triassic formations in the core of the anticline. Triassic dolostone and thickened gypsum/mudstone units are then considered as different polygons in 2.5D models. Justified by the variable proportion of dolomites and evaporites in the upper, competent Triassic unit, we use a range of density values (2300-2420 kg/m^3) that corresponds to 5%-33% of dolostones with respect to its whole thickness. Using these data, we can consider a range of possible gravity profiles in which both the overall trend and main

residual gravity lows are satisfied (see orange dashes lines in Fig. 5). For the Western Section, the DF model is characterized by a modeled gravity profile that reasonably fits the observed gravity in both amplitude and symmetry. Conversely, in the RA model, the overall modeled profiles are more asymmetric than the residual profiles.

In the Eastern Section, the modeled profile corresponding to the DF model shows a lower asymmetry than the residual gravity profile. Asymmetry of the modeled gravity in the RA model is more pronounced and consistent, although slightly shifted to the south, with the residual value.

6. DISCUSSION: GRAVITY MODELS AND STRUCTURES

The Bouguer and residual anomaly maps and the modeled cross-sections allow us to improve the knowledge of the geometry of the Santo Domingo Anticline and provide inputs that must be considered in future cross-sections and interpretations of this key structure. The obtained regional gravity anomaly is consistent with the northwards deepening of the Moho and shows a WNW-ESE trend (parallel to the trend of the Axial Zone) confirming the significant role played by basement thrusts in crustal thickening. Unexpectedly (considering an *a priori* large volume of Upper Triassic materials below the anticline), the resulting residual anomaly shows highs and lows of small amplitude. They are not clearly defined, continuous or aligned to the prominent topography of the core of the anticline which supports the existence of lateral variations in the structure at depth and therefore an along-strike change in the geometry of folds/thrusts.

Considering the symmetry of the anomaly that suggests the presence of a symmetric body at depth, the DF model better fits gravimetric data in the gravimetric profile of the Western Section. On the other hand, the asymmetry of the gravimetric profile of the Eastern

Section could be better modeled by an asymmetric structure similar to what expected by the RA model. However, in the Eastern Section, neither of the two end-member hypotheses properly fits with the residual value and therefore we propose a modified RA model (Fig. 5e), which falls into an intermediate option between the two end-members. The density of the Triassic rocks in our model is 2380 kg/m^3, intermediate between the measured values and corresponding with the best fit between the residual gravity curve and the model. .

The along-strike change in geometry suggested by our 2.5D models has important implications regarding the structures of the study area. Our modeled residual gravity profiles indicate a change moving from west to east from a detachment fold to a ramp anticline structure. Taking into account this along-strike change and the residual anomaly map (Fig. 3c), we can go one step further in the interpretation of the gravity anomalies. To the west of the Eastern Section (Fig. 3), the central, main gravity low shows a well-defined symmetry. Towards the east, this gravity low progressively becomes a doubled anomaly that breaks the symmetry and consists of a gravity high and a minor gravity low. The transition from a ramp anticline to a detachment fold has been previously suggested not far from this position by Millán *et al*., (1995) and Pueyo *et al*. (2004). These authors propose that the early formed footwall ramp would be subsequently folded and progressively involved in the southern flank of the anticline following a conical, non-coaxial geometry. From the interpretation of gravity anomalies and their 2.5D modeling, it is possible to locate more accurately the transition between the detachment fold that characterizes the Santo Domingo Anticline and the footwall ramp (and associated ramp anticline) characterizing the rest of the External Sierras front.

This abrupt change is located immediately west of the Eastern Section (Fig. 2a), and it is also coincident with the change in dip of the northern limb of the Santo Domingo anticline (shallower to the east, steeper to the west; Millán *et al*., 1995, their Fig. 3). Structural transition in geometry and dips is also related to the contrasting geometries and the associated

decrease of volume of low-density rock coring the anticline.

Finally, an important result derived from the gravimetric survey, the residual anomaly map and the modeled cross-sections suggests that density changes can occur within *a priori* simple, low-density homogeneous succession. Surface geology indicates in this case the presence of stratified bodies of dolostones within the Upper Triassic rocks. Therefore, the existence of these density variations can give some hints for the interpretation of gravity anomalies that otherwise would be neglected.

7. CONCLUSIONS

A new gravimetric survey was performed around the Santo Domingo Anticline with the aim of unraveling its controversial origin in relation to depth structures. A WNW-ESE elongated gravity low (-2.5 mGal) has been identified in the residual anomaly map in correspondence of the evaporites located in the core of the Santo Domingo Anticline. The western termination of the gravity low coincides with the periclinal end of the Santo Domingo Anticline whereas its eastern termination marks the transition from a detachment fold (with evaporites in its core) to a fault-related fold geometry. Gravity results allow positioning, with reasonable accuracy, the lateral and at depth switch from a ramp to a detachment fold under the Santo Domingo Anticline.

Acknowledgements

The authors thank help from project CGL2014-54118-C2 of the Ministerio de Economía y Competitividad and European Union ERFD funds. The authors acknowledge the support for this research provided by the Geotransfer Research Group (Aragón Government) and special thanks to Vicky Burriel, Elisa Sánchez, Belén Oliva and Miguel Gallego for field support.

Constructive support from R. Stephenson, Chiara Frassi and two anonymous reviewers helped to improve a former version of the manuscript.

References

Almela, A., Ríos, J.M. 1951. Mapa Geol. de España 1:50.000, serie antigua, hoja nº 248 (Apiés). I.G.M.E. Ed., Madrid: 94 pp., 1 map.

Anastasio, D. J. 1992. Structural evolution of the external Sierra, southern Pyrenees, Spain. In: *Structural Geology of Fold-and-Thrust Belts*, Mitra, S., Fisher, G.W. (eds). Johns Hopkins University Press: Baltimore; MD, 239-251.

Arenas, C. 1993. *Sedimentología y paleogeografía del Terciario del margen pirenaico y sector central de la Cuenca del Ebro (zona aragonesa occidental)*. Ph.D Thesis, Universidad de Zaragoza. 858 pp.

Arenas, C., Millán, H., Pardo, G., Pocoví, A. 2001. Ebro Basin continental sedimentation associated with late compressional pyrenean tectonics (NE Iberia): controls on margin fans and alluvial systems. *Basin Research* **13**; 65-89. DOI: 10.1046/j.1365-2117.2001.00141.x.

Ayala, C., Bohoyo, F., Maestro, A., Reguera, M. I., Torne, M., Rubio, F., Fernàndez, M., García-Lobón, J. L. 2016. Updated Bouguer anomalies of the Iberian Peninsula: a new perspective to interpret the regional geology. *Journal of Maps*, 1-4.

Barnolas, A., Gil-Peña, I. 2001. Ejemplos de relleno sedimentario multiepisódico en una cuenca de antepaís fragmentada: La Cuenca Surpirenaica. *Boletín Geológico y Minero* **112**: 17-38.

Beauchamp, W., Allmendinger, R. W., Barazangi, M., Demnati, A., El Alji, M., Dahmani, M. 1999. Inversion tectonics and the evolution of the High Atlas Mountains, Morocco, based on a geological□geophysical transect. *Tectonics* **18**, 163-184.

Casas, A., Kearey, P., Rivero, L., Adam, C.R. 1997. Gravity anomaly map of the Pyrenean region and comparison of the deep geological structure of the western and eastern Pyrenees. *Earth and Planetary Science Letters* **150**, 65-78. DOI: 10.1016/S0012-821X(97)00087-3.

Casas, A. M., Pardo, G. 2004. Estructura pirenaica y evolución de las cuencas sedimentarias en la transversal Huesca-Oloron. In: *Itinerarios geológicos por Aragón,* Colombo, F., Liesa, CL, Meléndez, G., Pocovi, A., Sancho, C., Soria AR (eds). Geo Guías (Sociedad Geológica de España) 1, 63-96.

Cousenz-Schultz, B.A., Vendeville, B.C., Wiltschko, D.V. 2003. Duplex style and triangle

zone formation: insights from physical modeling. *Journal of Structural Geology* **25**, 1623-1644. DOI: 10.1016/S0191-8141(03)00004-X.

Choukroune, P., ECORS team 1989. The ECORS Pyrenean deep seismic profile reflection data and the overall structure of an orogenic belt. *Tectonics* **8**, 23-39. DOI: 10.1029/TC008i001p00023.

Dahlstrom, C. D. A. 1969. Balanced cross sections. *Canadian Journal of Earth Sciences* **6**, 743-757.

Epard, J.L., Groshong, R.H. 1995. Kinematics model of detachment folding incluiding limb rotation, fixed hinges and layer-parallel strain. *Tectonophysics* **247**, 85-103. DOI: 10.1016/0040-1951(94)00266-C.

Fillon, C., Huismans, R.S., Van Der Beek, P. 2013. Syntectonic sedimentation effects on the growth of fold-and-thrust belts. *Geology* **41**, 83-86. DOI: 10.1130/G33531.1.

Gestain, V., Nalpas, T., Rouby, D., Barrier, L. 2004. Rôle des niveaux incompetents syncinématiques sur l'evolution des zones chevauchantes – modélisation analogique. *Bulletin de la Societe Geologique de France* **175**, 351-359. DOI: 10.2113/175.4.351.

Hammer, S. 1939. Terrain corrections for gravimeter stations. *Geophysics* **4**, 184–194. DOI: 10.1190/1.1440495.

Heiskanen, W. A., Moritz, H. 1969. Physical geodesy. W. H. Freeman Co.

Henkel, H. (1976). Studies of density and magnetic properties of rocks from northern Sweden. *Pure and applied geophysics* **114**, 235-249.

Hervouët, Y., Espurt, N., Dhont, D. 2005. Failles normales Paléocène à Lutétien en zone sud-pyrénéenne (Aragon, Espagne) et flexuration de la plaque ibérique. *Comptes Rendus Geoscience* **337,** 385–392. DOI: 10.1016/j.crte.2004.11.001.

Hinze, W.J., Aiken, C., Brozena, John., Coakley, B., Dater, D., Flanagan, G., Forsberg, R., Hildenbrand, T., Randy-Keller, G., Kellogg, J., Kucks, R., Li, X., Mainville, A., Morin, R., Pilkington, M., Plouff, D., Ravat, D., Roman, D., Urrutia-Fucugauchi, J.,Véronneau, M., Webring, M., Winester, D. 2005. New standards for reducing gravity data: The North American gravity database. *Geophysics* **70**, 125-132. DOI: 10.1190/1.1988183.

Hogan, P. J., Burbank D.W. 1996. Evolution of the Jaca piggyback basin and emergence of the External Sierra, southern Pyrenees. In: *Tertiary basins of Spain the stratigraphic record of crustal kinematics*, Friend, P.F., Dabrio, C.J. (eds). Cambridge University Press, 153-160.

Homza, T.X., Wallace, W.K. 1995. Geometric and kinematics models for detachment folds with fixed and variable detachment depths. *Journal of Structural Geology* **17**, 575-588. DOI: 10.1016/S0191-8141(96)00118-6.

Izquierdo-Llavall, E., Aldega, L., Cantarelli, V., Corrado, S., Gil-Peña, I., Invernizzi, Ch.

and Casas, A.M. 2013. On the origin of cleavage in the Central Pyrenees: Structural and paleo-thermal study. *Tectonophysics* **608**, 303-318. DOI: 10.1016/j.tecto.2013.09.027.

Jamison, W. R. 1992. Stress controls on fold thrust style. In: *Thrust tectonics*, McClay, K.R. (ed.). Springer: Netherlands, 155-164. DOI: 10.1007/978-94-011-3066-0_13.

Konstantinovskaya, E., Malavieille, J. 2011. Thrust wedges with décollement levels and syntectonic erosion: a view from analoque models. *Tectonophysics* **502**, 336-350. DOI: 10.1016/j.tecto.2011.01.020.

Labaume, P., Séguret, M., Seyve, C. 1985. Evolution of a turbiditic foreland basin and analogy with an accretionary prism: Example of the Eocene South-Pyrenean basin. *Tectonics* **4**, 661-685. DOI: 10.1029/TC004i007p00661.

LaFehr, T. R. 1991. Standardization in gravity reduction. *Geophysics* **56**, 1170–1178. DOI:10.1190/1.1443137.

Lohrmann, J., Kukowski, N., Adam, J., Oncken, O. 2003. The impact of analogue material properties on the geometry, kinematics, and dynamics of convergent sand wedges. *Journal of Structural Geology* **25**, 1691–1711. DOI: 10.1016/S0191-8141(03)00005-1.

Mallada, L., 1878. *Descripción física y geológica de la provincia de Huesca*. Memorias Completas del Mapa Geológico de España, Madrid.

Martínez-Peña, M., Casas-Sainz, A. 2003. Cretaceous–Tertiary tectonic inversion of the Cotiella Basin (southern Pyrenees, Spain). *International Journal of Earth Sciences* **92**, 99-113. DOI: 10.1007/s00531-002-0283-x.

McClay, K.R., Whitehouse, P. 2004. Analogue modelling of doubly vergent thrust wedges. In: *Thrust Tectonics and Hydrocarbon Systems*, McClay, K.R. (ed.). American Association of Petroleum Geologists Memoir, 184–206.

McElroy, R. 1990. *Thrust kinematics and syntectonic sedimentation: the Pyrenean frontal ramp, Huesca, Spain.* Unpublished Ph.D Thesis, University of Cambridge. 175.

Massoli, D., Koyi, H.A., Barchi, M.R. 2006. Structural evolution of a fold and thrust belt generated by multiple décollements: analogue models and natural examples from the Northern Apennines (Italy). *Journal of Structural Geology* **28**, 185-199. DOI: 10.1016/j.jsg.2005.11.002.

Millán, H., Pocoví, A., Casas, A. 1995. El frente de cabalgamiento surpirenaico en el extremo occidental de las Sierras Exteriores: sistemas imbricados y pliegues de despegue. *Revista de la Sociedad Geológica de España* **8**, 73-90.

Millán, H., 1996. *Estructura y cinemática del frente de cabalgamiento surpirenaico en las Sierras Exteriores Aragonesas*. Ph.D Thesis, Universidad de Zaragoza. 330 pp.

Millán, H., Pueyo, E.L., Aurell, M., Luzón, A., Oliva, B., Martínez, M.B., Pocoví, A. 2000. Actividad tectónica registrada en los depósitos terciarios del frente meridional del

Pirineo central. *Revista de la. Sociedad Geológica de España* **13**, 279-300.

Mitra, S. 1990. Fault-Propagation folds: geometry, kinematic evolution and hydrocarbon traps (1). *AAPG Bulletin* **74**, 921-945.

Mochales, T., Casas, A.M., Pueyo, E.L., Barnolas, A., 2012. Rotational velocity for oblique structures (Boltaña anticline, Southern Pyrenees). *Journal of Structural Geology* **35**, 2–16. DOI:10.1016/j.jsg.2011.11.009.

Moritz, H. 1980. Geodetic Reference System 1980. *Bulletin Géodésique* **54**, 395-405. DOI: 10.1007/BF02519014.

Muñoz, J.A. 1992. Evolution of a Continental Collision Belt: ECORS-Pyrenees Crustal Balanced Cross-section. In: *Thrust tectonics*, McClay, K.R. (ed.). Springer: Netherlands, 235-246. DOI: 10.1007/978-94-011-3066-0_21.

Mutti, E., Seguret, M., Sgavetti, M. 1988. Sedimentation and deformation in the Tertiary sequences of the Pyrenees: Field Trip 7 Guidebook. *AAPG Mediterranean Basin Conference, Nice, France*, Special Publication of the Institute of Geology of the University of Parma.

Nichols, G.J. 1984. *Thrust tectonics and alluvial sedimentation, Aragón, Spain.* Unpublished Ph D. Thesis, University of Cambridge. 243 pp.

Nichols, G. J., 1987. The Structure and Stratigraphy of the Western External Sierras of the Pyrenees, Northern Spain. *Geological Journal* **22**, 245-259. DOI: 10.1002/gj.3350220307.

Nilfouroushan, F., Pysklywec, R., Cruden, A.R., 2011. Sensitivity analysis of numerical scaled models of fold-and-thrust belts to granular material cohesion variation and comparison with analogue experiments. *Tectonophysics* **526-529**, 196-206. DOI: 10.1016/j.tecto.2011.06.022.

Oliva-Urcia, B, Beamud, E., Garcés, M., Arenas, C., Soto, R., Pueyo, E.L., Pardo, G. 2016. New magnetostratigraphic dating of the Paleogene syntectonic sediments of the West-Central Pyrenees: Tectonostratigraphic implications. In: P*alaeomagnetism in fold-and-thrust belts; new perspectives*. Pueyo, E.L., Cifelli, F., Sussman, A.J., Oliva-Urcia, B. (eds.). Geological Society Special Publication.

Ori, G.G., Friend, P.F. 1984. Sedimentary basins fromed and carried piggyback on active thrust sheets. *Geology* **12**, 475-478. DOI: 10.1130/0091-7613(1984)12<475:SBFACP>2.0.CO;2.

Pedley, R.C, Busby, J.P., Dabek, Z.K. 1993. *GRAVMAG User Manual - Interactive 2.5D gravity and agnetic modelling*. British Geological Survey, Technical Report WK/93/26/R.

Pinto, V., Casas, A. 1996. An interactive 2D and 3D gravity modeling program for IBM-compatible personal computers. Compututers and Geosciences **22**, 535– 546. DOI: 10.1016/0098-3004(95)00125-5.

Pueyo E. L., Pocoví, A., Millán, H., Sussman, A.J. 2004. Map view model to correct and calculate shortening in rotated thrust fronts using paleomagnetic data. In: *Paleomagnetic and structural analyses of orogenic* curvature. Sussman, A.J.,Well, A.B., (eds.). Geological Society of America Spec. Publ. 383, 57-71. DOI: 10.1130/0-8137-2383-3(2004)383[57:MMFCAC]2.0.CO;2.

Puigdefàbregas, C. 1975. La sedimentación molásica en la cuenca de Jaca. *Pirineos* **104,** 1-188.

Puigdefàbregas, C., Soler, M. 1973. Estructura de las Sierras Exteriores pirenaicas en el corte del río Gállego. (prov. de Huesca). *Pirineos* **109**, 5-15.

Puigdefàbregas, C., Souquet, P. 1986. Tecto-sedimentary cycles and depositional sequences of the Mesozoic and Tertiary from the Pyrenees. *Tectonophysics* **129**, 173-203. DOI: 10.1016/0040-1951(86)90251-9.

Richard, P., Cobbold, P.R. 1989. Structures en fleur positives et décrochements crustaux: modélisation analogique et interprétation mécanique. *Comptes rendus de l'Académie des sciences. Série II* **308**, 553–560.

Rodríguez-Pintó, A., Pueyo, E.L., Calvín, P., Sánchez, E., Ramajo, J., Casas, A.M., Ramón, M.J., Pocoví, A., Barnolas, A., Román, T., 2016. Rotational kinematics of a curved fold: The Balzes anticline (Southern Pyrenees). *Tectonophysics* **677**, 171–189. DOI:10.1016/j.tecto.2016.02.049

Santolaria, P., Casas-Sainz, A.M., Soto, R., Pinto, V., Casas, A. 2014. The Naval diapir (Southern Pyrenees): Geometry of a salt wall associated with thrusting at an oblique ramp. *Tectonophysics* **637**, 30-44. DOI: 10.1016/j.tecto.2014.09.008.

Sarsar-Naouali, B., Inoubli, M.H., Amiri, A., Chaqui, A., Hamdi, I. 2011. Subsurface geology of the Ariana región (Diapir Zone, northern Tunisia) by means of gravity analysis. Geophysical Prospecting, **59**, 983-997. DOI: 10.1111/j.1365-2478.2011.01004.x

Séguret, M. 1972. *Etude tectonique des nappes et series decollées de la partie centrale du versant sud des Pyrenées. Caractère sédimentaire, rôle de la compression et de la gravité*. Ph.D Thesis, Université des Sciences et Techniques du Languedoc (Montpellier II), Sér. Geol. Struct. nº 2. 155 pp.

Sheriff, R. E., Geldart, L. P. 1995. *Exploration seismology,* Cambridge University Press, 628 pp.

Smit, J.H.W., Brun, J.-P., Soukoutis, D. 2003. Deformation of brittle–ductile thrust wedges in experiments and nature. *Journal of Geophysical Research* **108**, 2480

Soto, R., Casas, A. M., Storti, F., Faccenna, C. 2002. Role of lateral thickness variations on the development of oblique structures at the Western end of the South Pyrenean Central Unit. *Tectonophysics* **350**, 215-235. DOI: 10.1016/S0040-1951(02)00116-6.

Soto, R., Storti, F., Casas, A. M., Faccenna, C. 2003. Influence of along-strike pre-orogenic

sedimentary tapering on the internal architecture of experimental thrust wedges. *Geological magazine* **140**, 253-264. DOI: 10.1017/S0016756803007817.

Soto, R., Casas-Sainz, A.M. Pueyo, E.L. 2006. Along-strike variation of orogenic wedges associated with vertical axis rotations. *Journal of Geophysical Research (Solid Earth)* **111**, B10402 – B10423. DOI:10.1029/2005JB004201.

Suppe, J. 1983. Geometry and kinematics of fault-bend folding. *American Journal of Science* **283**, 684-721. DOI: 10.2475/ajs.283.7.684.

Suppe, J., Medwedeff, D.A. 1990. Geometry and kinematics of fault propagation folding. *Eclogae geologicae Helvetiae* **83**, 409-454.

Teixell, A., García Sansegundo, J. 1995. Estructura del sector central de la Cuenca de Jaca (Pirineos meridionales). *Revista de la Sociedad Geológica de España* **8**, 215-228.

Teixell, A. 1996. The Ansó transect of the southern Pyrenees: basement and cover thrust geometries. *Journal of the Geological Society*, **153**, 301-310.

Teixell, A. 1998. Crustal structure and orogenic material budget in the west central Pyrenees. *Tectonics* **17**, 395-406. DOI: 10.1029/98TC00561

Turner, J.P. 1988. *Tectonic and stratigraphic evolution of the West Jaca thrust-top basin, southwestern Pyrenees*. Unpublished Ph.D. thesis, University of Bristol.

Turner, J. P. 1992. Evolving alluvial stratigraphy and thrust front development in the West Jaca piggyback basin, Spanish Pyrenees. *Journal of the Geological Society* **149**, 51-63. DOI: 10.1144/gsjgs.149.1.0051.

Tziavos, I.N., Vergos, G.S., Grigoriadis, V.N. 2010. Investigation of topographic reductions and aliasing effects on gravity and the geoid over Greece based on various digital terrain models. *Surveys in Geophysics* **31**, 23-67. DOI: 10.1007/s10712-009-9085-z.

Vaquero, P.A., Sainz-Maza, S. 2011. *Reseña de punto destacado de gravimetría absoluta, Red Española de Gravimetría Absoluta*, IGN, pp. 2.

Woodward, N.B., Boyer, S.E., Suppe, J. 1991. *Balanced geological cross-sections: an essential technique in geological research and exploration.,* pp. 132 DOI: 10.1029/SC006.

Table 1. Laboratory density vaules (ρ), number of sampled measured (n), mean, mode and standard deviation of the different litostratigraphic units.

Lithostratigraphic Unit	Age	Lithology	Density (Kg/m^3)			
			n	mean	mode	standard deviation
Keuper Facies	Upper Triassic	Evaporites and shales	141	2282	2250-2275	0.192
Adraen-Bona Fm.	Upper Cretaceous	Limestones	85	2670	2675-2700	0.057
Guara Fm.	Middle Eocene	Limestones	25	2646	2625-2650	0.058
Arguis Fm.	Middle-Upper Eocene	Marls	49	2533	2550-2575	0.119
Campodarbe Fm.	Upper Eocene-Oligocene	Sandstones	41	2634	2650-2675	0.057
		Shales	34	2578	2575-2600	0.046
		All	101	2612	2625-2650	0.057
Uncastillo Fm.	Lower Miocene	Molasse	59	2390	2325-2350	0.16

Table 2. Physical properties of polygons used in the 2.5D gravity modeling (Fig. 5). Half Strike indicates the half-length of the bodies perpendicular to the profile. Δρ = ρ polygon – ρ background, being ρ background = 2560 Kg/m^3.

Polygon number	Lithostratigraphics units	Δρ (Kg/m^3)	Half Strike (m)
1	Paleozoic basement	110	10000
2	Triassic	-260	10000
3	Cretaceous-Eocene Limestones	100	10000
4	Eocene marls	-20	10000
5	Syntectonic continental Cenozoic	27	10000
6	Post-tectonic continental Cenozoic	-55	10000

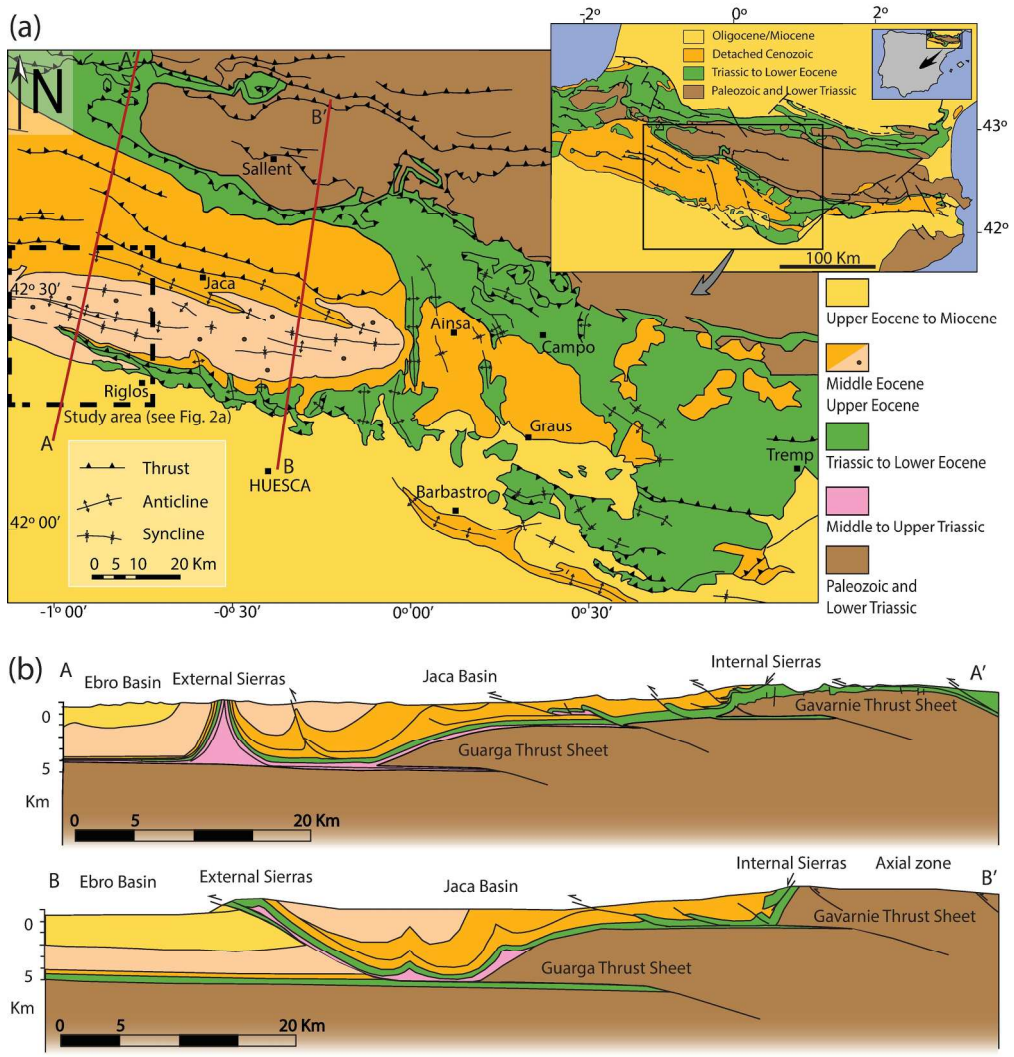

Figure 1. a) Geological sketch of the southern portion of the Pyrenees between the Axial Zone, in the north, and the Ebro foreland Basin, in the south. Note the presence of long, Pyrenean WNW-ESE structures superimposed on shorter, NNW-SSE structures. Location of the study area and the traces of the two geological cross-sections are also shown. b) Geological cross-sections across the External Sierras. Note the different structures developed along the External Sierras front.

Fig. 1

208x219mm (300 x 300 DPI)

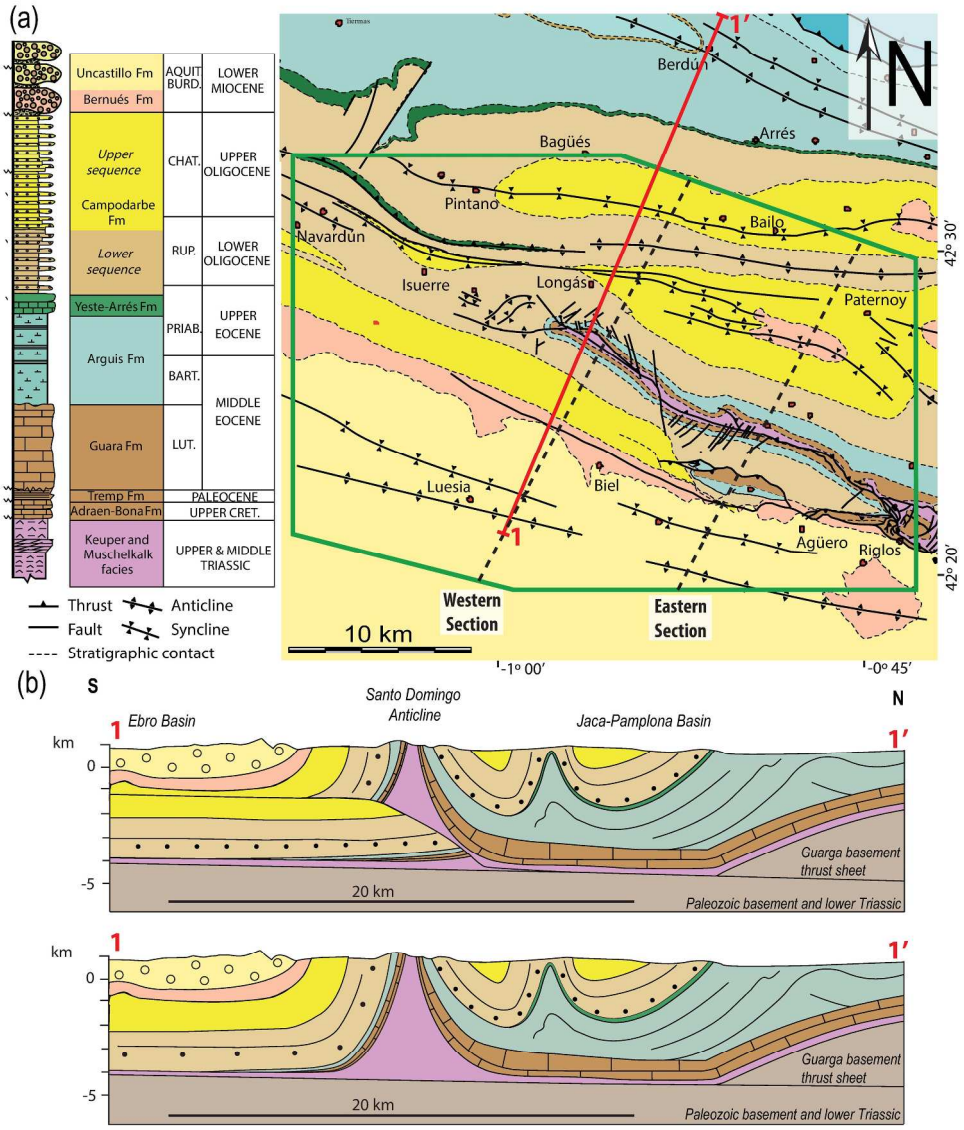

Figure 2. a) Geological map and synthetic stratigraphic column of the study area (modified from Puigdefábregas, 1975; Millan, 1996; Pueyo, 2000). Green line defines the aerial extension of the gravity maps shown in Fig. 3. Dash black lines are the traces of the cross-sections showed in Fig. 5. b) Geological cross-sections (along the 1-1′ section) of the Santo Domingo Anticline showing the two possible interpretations of the depth structures. The upper cross-sections shows a ramp anticline (RA model) (modified from Teixell and García-Sansegundo, 1995) and the second one a detachment fold (DF model) (modified from Teixell and García-Sansegundo, 1995, after Millán et al., 1995).

Fig. 2

251x300mm (300 x 300 DPI)

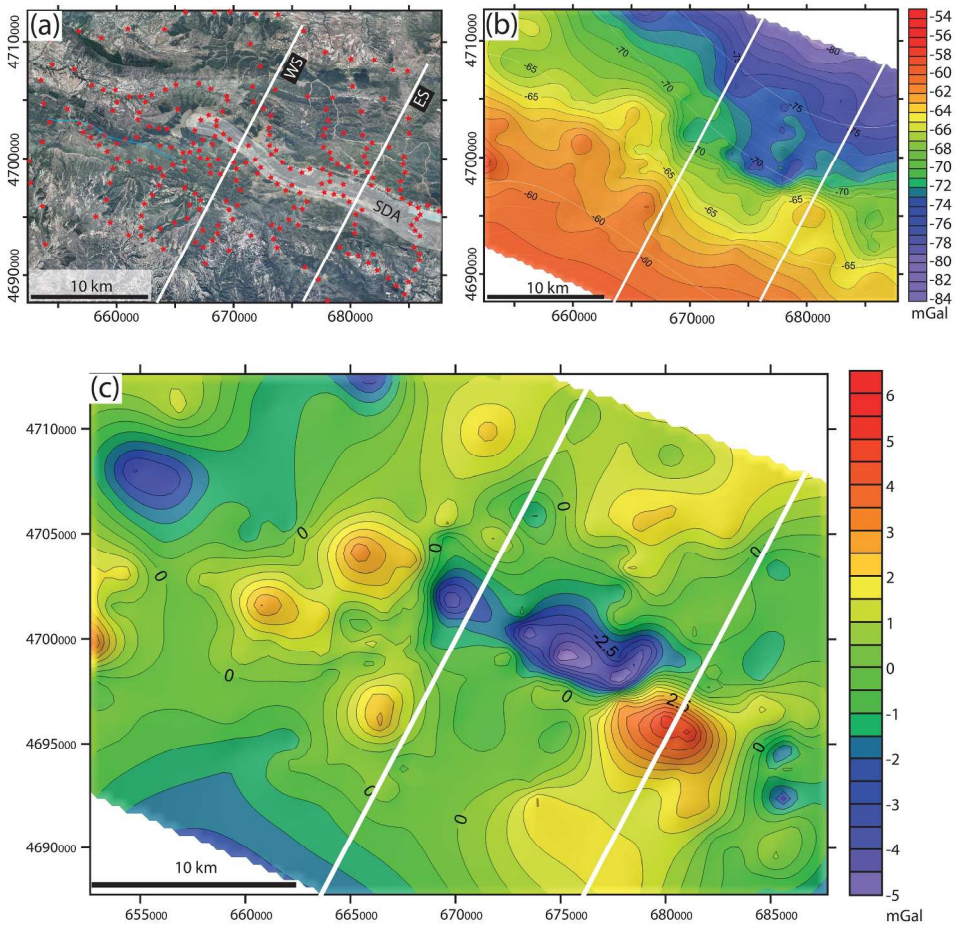

Figure 3. a) Orthophotograph of the study area showing the positions of the gravity stations and cross-sections (WS: Western Section; ES: Eastern Section; PNOA obtained from © Instituto Geográfico Nacional). Santo Domingo Anticline is shaded in white (SDA). b) Bouguer anomaly map (colored map and black lines) and regional gravimetric map (white thin lines). c) Residual anomaly map obtained by the subtraction of the regional gravimetric anomaly from the Bouguer anomaly map. UTM coordinates (30T zone and ETRS89 datum; EPGS:6258). Straight white lines in "b)" and "c)" correspond with the Western and Eastern Sections, respectively.

Fig. 3

225x242mm (300 x 300 DPI)

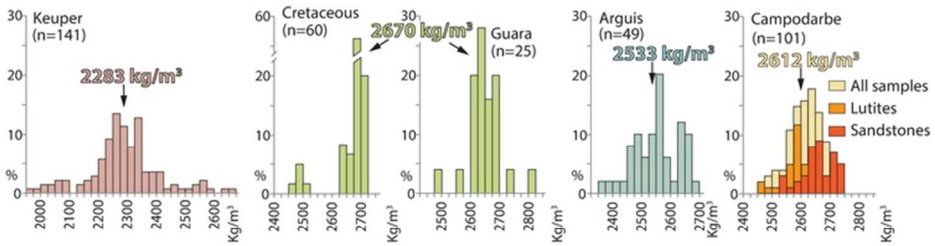

Figure 4. Frequency charts of the laboratory density values of main litostratigraphic units of the Santo Domingo Anticline area. Percentages are relative to data from each lithostratigraphic unit.
Fig. 4
68x22mm (300 x 300 DPI)

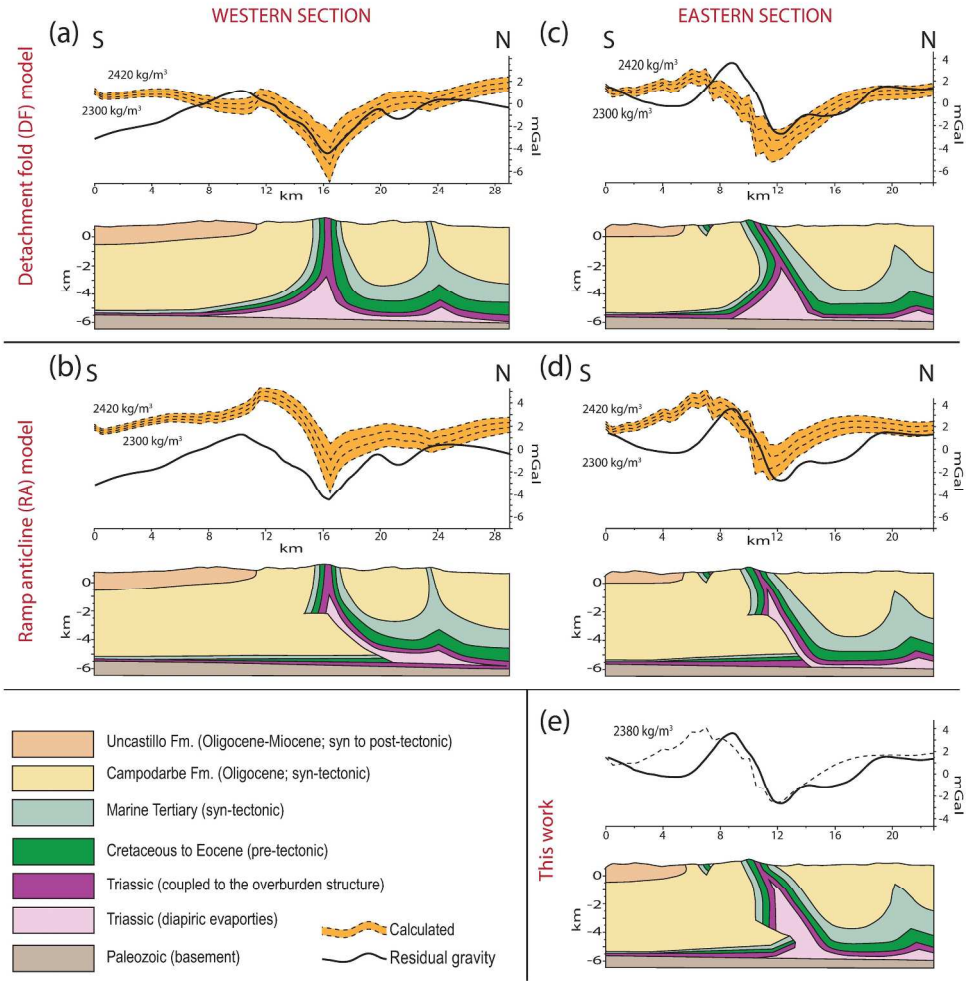

Figure 5. 2.5D Gravity models and associated geological cross-sections for the two possible interpretations proposed for the study area. a) and b) Detachment fold (DF) model along the Western and Eastern Sections, respectively. c) and d) Ramp anticline (RA) model along the Western and Eastern Sections, respectively. Orange strip is related to the uncertainty in the density of the Upper Triassic, between 2300 and 2420 kg/m^3 (see text); dashed lines show the modeled signal for intervals of 40 kg/m^3 (see text for details). d) New model proposed in this work for the Eastern Section (density of the Upper Triassic: 2380 kg/m^3 -see text for further explanations-). See Fig. 2 for the location of the geological cross-sections.

Fig. 5

250x297mm (300 x 300 DPI)

Figure 6. Aerial photograph (looking to the east) of the study area showing the core and northern limb of the Santo Domingo Anticline. The ductile Triassic units (Upper Triassic and M2) and the Triassic dolostones (M3) coupled to the overburden at the limbs of the anticline can be distinguished.
Fig. 6
156x116mm (300 x 300 DPI)